

# Star formation in bar environments<sup>\*</sup>

## II. Physical properties, age and abundances of H II regions

P. Martin<sup>1</sup> and D. Friedli<sup>2</sup>

<sup>1</sup> Canada-France-Hawaii Telescope, PO Box 1597, Kamuela, HI 96743, USA. E-mail: martin@cfht.hawaii.edu

<sup>2</sup> Geneva Observatory, CH-1290 Sauverny, Switzerland. E-mail: Daniel.Friedli@obs.unige.ch

Received: March 15, 1999; accepted: April 8, 1999

**Abstract.** The nebular properties (electronic density, extinction, age, O/H abundances) of H II regions found along the bars of the sample of barred spiral galaxies studied by Martin & Friedli (1997) are examined. From line ratio diagnostic diagrams, it is showed that regions located along the major axis of the bars have a normal photoionization spectrum, that is, line ratios reproducible from nebular conditions and ionizing star radiation field normally encountered in extragalactic H II regions. There is an indication, however, that their degree of ionization might be somewhat different. Another ionization mechanism (high-velocity shocks or hard UV radiation) is clearly present for regions found nearby the centers of the galaxies. The electronic density of the regions along the bars is very close to that of disc regions ( $\langle N_e \rangle \sim 80 \text{ cm}^{-3}$ ). On average, bar and disc regions have a similar visual extinction ( $A_V \sim 1 \text{ mag}$ ) with exceptions for some regions located near the bar dust lanes of the earlier types of galaxies in our sample. Although the average H $\alpha$  equivalent width of bar H II regions ( $\sim 250 \text{ \AA}$ ) is half that of disc regions, this disparity could be due to uncertainties in the galactic continuum and does not translate into a significant age difference. The oxygen abundance distribution was also investigated in the bar of these galaxies. The O/H scatter was found to be very small ( $< 0.1 \text{ dex}$ ) indicating that mixing of the chemical composition by gas flows is very efficient in a barred structure.

**Key words:** Galaxies: abundances – Galaxies: ISM – Galaxies: spiral – Galaxies: starburst – Galaxies: kinematics and dynamics – ISM: H II regions

### 1. Introduction

Galactic bars are the sites of highly diversified star formation activities. Phillips (1993, 1996), García-Barreto et al. (1996) and Martin & Friedli (1997, hereafter MF97) have all showed that *along* certain bars, mostly found in late-type spirals, star formation (SF) can be quite intense. For instance, the bar of the SBcd galaxy NGC 4731 has a total star formation rate (SFR) of about  $1.5 M_{\odot} \text{ yr}^{-1}$  (MF97). However, in other cases, SF in the bar can be very weak or completely absent. This is the case for most of the bars in early-type barred spirals (e.g. NGC 1300, NGC 1512, NGC 3351). The origin of these differences is not yet completely understood. Numerical simulations (Friedli & Benz 1995, MF97, Martinet & Friedli 1997) and observations (Martin & Roy 1995) suggest that the existence of massive star formation in certain bars is a relatively brief event ( $\sim 0.5\text{--}1.0 \text{ Gyr}$ ) in the evolution of a barred system and that it mostly takes place during the formation of the bar itself. The amplitude and duration of the event is, however, controlled by a complicated combination of different physical processes. For example, the time-dependent bar evolution, initial gas content, amplitude of gas flows, and mechanical energy injected in the interstellar medium (ISM) by supernovae ejecta are all factors that can influence the level of SF activity in bars (MF97). Hence, it is essential to acquire more data on the properties of the H II regions formed in such environments to better constrain the relative importance of these factors, and consequently significantly improve SF recipes used in numerical simulations.

The morphology, SFRs and other properties of SF along the bars of a sample of eleven spiral galaxies were studied in the first paper in this series (MF97). Including the large diversity in SF activity, MF97 found that the distribution of H II regions can be highly asymmetrical in the bar. For some SBc spirals, large regions can be present outside the bar major axis. This morphology suggests that the SF process along the bar of late-type spirals is a chaotic process, not strictly confined along the major stellar/gas orbits defined by the barred potential. In such a case, one could expect similar properties for these H II

---

Send offprint requests to: P. Martin

<sup>\*</sup> Observations reported in this paper were obtained at the Multiple Mirror Telescope Observatory, a facility operated jointly by the University of Arizona and the Smithsonian Institution

regions when compared to the disc star forming regions. The situation could be different for bars in earlier types of galaxies for which the star forming regions are generally located next to dust lanes (MF97). For one galaxy of their sample (NGC 7479), MF97 also estimated the amount of gas flowing in the bar and falling into the galaxy center. They found that possibly as much as 75% of the gas in the bar is not transformed into stars. Numerical simulations suggest that this number is very dependent on the presence of bar-induced shocks in the star forming ISM. It is then critical to determine whether there is some signature of these shocks in the H II regions along the bars.

In this paper, spectrophotometric data are used to derive the physical properties of a sub-sample of H II regions found along the bars of the galaxies studied by MF97. As a comparison sample, a few regions located in the discs of these galaxies have also been analysed. Using different diagnostic line ratio diagrams as defined by Baldwin et al. (1981) and Veilleux & Osterbrock (1987), the excitation of regions located in bar environments is compared to that of “normal” disc regions (Sect. 3.1). A similar analysis is performed for the electronic density using the appropriate sulfur line ratio (Sect. 3.2). The distributions of the visual extinction for both populations are also studied in Sect. 3.3. Using the H $\alpha$  equivalent width indicator (e.g. Leitherer et al. 1999), we also infer the approximate age of H II regions (Sect. 3.4). Since large-scale mixing of the chemical composition by bar-driven gas radial flows occurs in galaxy discs (Martin & Roy 1994; Friedli et al. 1994), the O/H distribution in bar environments is also investigated (Sect. 3.5).

## 2. Database

### 2.1. Observations

The long slit observations were conducted during two runs in April and October 1994 at the equivalent 4.5 meter Multi-Mirror Telescope on Mt Hopkins, Arizona. The “Blue Channel” spectrograph was used with a Loral 3k $\times$ 1k CCD. A grating with 500 grooves/mm and a blaze at 5410 Å was employed; the spectral range covered in the reduced spectra is about 3500 Å ( $\sim$ 3500  $\rightarrow$   $\sim$ 7000) with a dispersion of 1.17 Å/pixel. An order sorting filter was used (UV-36) and all the data were obtained with the CCD binned by a factor of two in the spatial direction (0.6''/pixel). All these observations were carried out with an unvignetted 2'' $\times$ 150'' slit positioned close to the parallactic angle to avoid any light loss. Three exposures of 15 or 20 minutes were obtained for each slit position in the bar. Between exposures, the alignment of the MMT six mirrors was verified and corrected, if necessary. Numerous standard stars were observed with a larger slit (5'') during the night for the flux calibration procedure.

Table 1 presents the journal of observations for the H II regions of ten of the eleven objects studied by MF97

(NGC 5068 was not observed). For some objects, a few slit positions were required to optimize the number of H II regions observed in the bar and the disc. Average seeing during these observations was about 1.2'' and conditions were photometric. Note that the only galaxy in the sample considered as an AGN (LINER) is NGC 7479.

### 2.2. Data reduction and analysis

The long slit spectra were reduced following standard procedures available in the LONGSLIT package in IRAF<sup>1</sup>. First, a bias and flat-field correction was applied. The illumination pattern along the slit was corrected using a set of sky flat-fields taken in the same optical configuration. Wavelength calibration was done using a Helium–Neon–Argon exposure taken immediately after the science observation. Geometric distortion and alignment of the spectra were corrected by 2D-mapping of the spectral lines from the calibration sources using the FITCOORDS and TRANSFORM algorithms.

The next step, sky subtraction, was done by extracting a sky background using sections along the long slit outside the galaxy. To make sure that the signal from the galaxy was minimized, the average sky backgrounds were compared between the different slit positions since most of the slits used for the disc H II regions were less contaminated by the disc emission. The spectra were then flux calibrated using a sensitivity function obtained from a set of standard stars observed through the nights. Extraction of the spectrum for each H II region was done using the spatial profile at H $\alpha$  seen along slit. In general, no continuum trace was found for these H II regions. The extraction trace was forced across the spectral range using the positions of the main nebular lines along the spectral domain. Finally, the individual spectra were combined.

The integrated fluxes of the main nebular lines H $\beta$ , [O II]  $\lambda$ 3727, [O III]  $\lambda\lambda$ 4959, 5007, [O I]  $\lambda$ 6300, [N II]  $\lambda$ 6584, H $\alpha$ , and [S II]  $\lambda\lambda$ 6717, 6731 were measured using a Gaussian fitting algorithm available with SPLIT in IRAF. A background continuum estimated from each side of the lines was automatically subtracted.

Many H II regions in bars show a strong underlying Balmer absorption at H $\beta$ . McCall et al. (1985) have shown that adding about 2 Å of equivalent width for normal disc regions constitutes an appropriate correction. This correction was applied for all the H $\beta$  fluxes for the H II regions in our control sample and the bar regions with shallow underlying absorption. However, for about 20% of the bar sample, this correction was not sufficient. For these regions, mostly located in the bars with a strong continuum (e.g. NGC 3504, NGC 5921, NGC 7479), the amplitude of

<sup>1</sup> IRAF is distributed by the National Optical Astronomy Observatories, which are operated by the Association of Universities for Research in Astronomy, Inc., under cooperative agreement with the National Science Foundation

**Table 1.** Journal of observations.

Galaxy	Epoch	# Slits	Slit PA [°]	Exposure Times [s]	<Airmass>	$N_{\text{bar}}^a$	$N_{\text{disc}}^a$	$L_{\text{bar}}^b$ [kpc]
NGC 1073	1994 Oct 9	1	68	3 × 1200	1.2	2	2	5.0
NGC 1087	1994 Oct 9	1	139	3 × 1200	1.4	2	2	1.6
NGC 3319	1994 Apr 17	1	40	1 × 1200	1.0	2	3	4.0
NGC 3359	1994 Apr 16	1	26	3 × 1200	1.2	8	5	5.8
NGC 3504	1994 Apr 16	2	140; 175	2 × 3 × 900	1.1	6	7	6.8
NGC 4731	1994 Apr 16	1	126	3 × 900	1.3	6	4	15.2
NGC 4900	1994 Apr 16	1	145	3 × 900	1.3	4	6	3.4
NGC 5921	1994 Apr 16	1	159	3 × 1200	1.2	5	4	8.1
NGC 7479	1994 Oct 4	2	2; 11	2 × 3 × 1200	1.3	7	9	16.6
NGC 7741	1994 Oct 4	2	92; 98	2 × 3 × 1200	1.1	7	1	3.5

<sup>a</sup> Number of bar and disc H II regions with detected H $\beta$ .

<sup>b</sup> Total length of the bar based on distance and measurements given in MF97.

the underlying absorption was estimated from a Gaussian fit. In general, we found that about 5 Å of equivalent width were necessary to assure a good correction. This value was applied for all bar regions with absorption higher than normal.

All of the line fluxes were corrected for interstellar reddening by comparing the H $\alpha$ /H $\beta$  ratio to the theoretical Balmer decrement (2.86) for Case B recombination (that is, for nebulae with large optical depths for the H I resonance lines) at 10<sup>4</sup> K. In reality, the temperature of bar H II regions is probably around 7000–8000 K due to their high O/H abundances (see below) so that our extinction based on the Balmer decrement might be overestimated by about 0.1 mag. Since the Balmer ratio represents only an approximation of the real extinction, we did not take this difference into account. The reddening law formulated by Savage & Mathis (1979) was assumed for reddening correction.

It is generally difficult to evaluate the accuracy of the absolute spectrophotometric fluxes for individual objects. The main uncertainties include the contamination by the bright galactic continuum, the underlying absorption at H $\beta$ , the accuracy of the photometric calibration, the spectrum extraction in a crowded field of H II regions, the positioning of the slit, the correction for the interstellar extinction and, of course, the intensity of the lines. We evaluate the accuracy of the fluxes to be at about 20–30%. Since we will only compare the global behavior of H II regions, these high uncertainties should not influence our conclusions.

### 3. Nebular properties

#### 3.1. Excitation

The basic source of ionization in an H II region is the UV radiation field from young massive stars. The emission line spectra resulting from a pure photoionization field in a Strömgren sphere can be studied using diagnostic diagrams (Baldwin et al. 1981; Evans & Dopita 1985; Veilleux & Osterbrock 1987; Osterbrock 1989; Dopita & Sutherland 1995; Rola et al. 1997). These standard diagrams

are based on nebular line ratios like [O III]/H $\beta$ , [O I]/H $\alpha$ , [N II]/H $\alpha$ , and [S II]/H $\alpha$ . For high redshift galaxies, the red part of the spectrum is shifted to the near-infrared. If optical studies are needed, other diagnostic lines like [O II]  $\lambda$ 3727 or [Ne III]  $\lambda$ 3869 can also be relied upon (Rola et al. 1997). These diagnostic diagrams are extremely useful in distinguishing between normal photoionized regions and regions with another ionization mechanism (e.g. high-velocity shocks, hard UV fields). The line ratios above are also independent of the reddening correction and depend only on the accuracy achieved for the spectrophotometry. However, despite the usefulness of these diagnostic diagrams for determining whether another ionization mechanism is present or not, it is very difficult to identify this mechanism. For this, sophisticated nebular models must be used (e.g. Stasińska 1990; Dopita & Sutherland 1995).

Figure 1 illustrates the first diagnostic diagram with a correlation between [O III]/H $\beta$  and [N II]/H $\alpha$  for the bar regions (dark symbols) and the disc regions of our control sample (open symbols). The dotted lines define the limits of the sequence of normal H II regions that can be found in Osterbrock (1989) and Kennicutt et al. (1989). The full line is the separation between normal photoionized regions and regions with another ionization mechanism. We have also indicated the effect of high-velocity shocks and magnetic fields on these line ratios from models by Dopita & Sutherland (1995). The average location of Seyfert 2 and LINER galaxies in this diagram are also displayed. At this time, it is still not entirely clear that the spectral characteristics (mainly the high [N II]/H $\alpha$  ratio) of these last objects are due to high UV radiation or high-velocity shocks (see discussion by Dopita & Sutherland 1995). However, Fig. 1 shows that excepting for four regions, *all the H II regions in our sample are located inside the sequence of normal H II regions*. These four regions are located close to the nucleus in NGC 3504 (a starburst galaxy) and NGC 7479 (LINER). Thus, from this diagram alone, bar H II regions do not exhibit any sign of high-velocity shocks or hard-UV radiation. Apart from these central peculiarities, there is no dependence on radius.

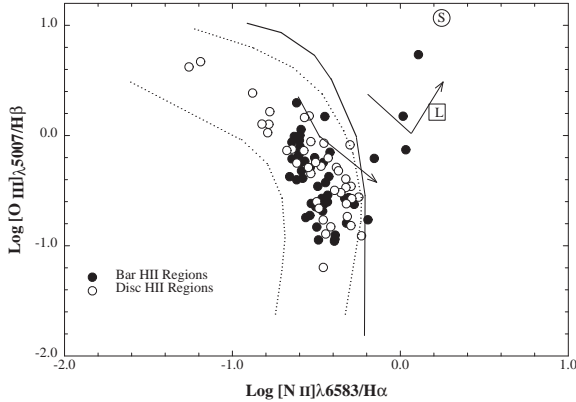


**Fig. 1.** Diagnostic diagram of our sample of bar and disc H II regions based on Osterbrock (1989). The sequence of normal regions is represented by the dotted lines. The full line indicates the separation between normal regions and regions with another ionization mechanism. The squared and circular symbols correspond to the average location of Seyfert 2 and LINER galaxies from Rola et al. (1997). The arrow lines indicate the effect of high-velocity shocks and magnetic fields on the line ratios from models by Dopita & Sutherland (1995). From the beginning to the end of the arrow, the velocity for the shock varies from 150 to 500 km s<sup>-1</sup>. The magnetic field parameter is zero for the bottom arrow and 4 μG cm<sup>3/2</sup> for the top arrow

Although [N II]/Hα is a good diagnostic ratio for high-velocity shocks or very hard ultraviolet radiation (Veilleux & Osterbrock 1987; Dopita & Sutherland 1995), other ratios like [S II]/Hα or [O I]/Hα are more sensitive to these ionization mechanisms. Figure 2 illustrates another diagnostic diagram: the correlation between [O III]/Hβ and [S II]/Hα. The dashed and full lines are as in Fig. 1. Arrows also show the effect of the high-velocity shocks and magnetic fields. Although most of the H II regions fall within the normal region sequence, there is a small number of bar regions outside the sequence. Figure 3 shows the sequence between [O III]/Hβ and [O I]/Hα. The latter ratio was detected in about 67% of the sample of bar regions but only in about 40% of the disc region sample.

From these diagrams, it is clear that *most bar H II regions do not exhibit any systematic evidence of high-velocity shocks (>150 km s<sup>-1</sup>) or very hard UV radiation*. Only circumnuclear regions exhibit obvious signs of another ionization mechanism (fast shocks and/or hard-UV radiation), as expected from the work of Kennicutt et al. (1989). Nevertheless, if these conditions do not appear to be present in bar regions, Figs. 2 and 3 suggest that shocks with lower velocity or an abnormal UV photoionization field cannot be excluded. This possibility is discussed in Sect. 4.

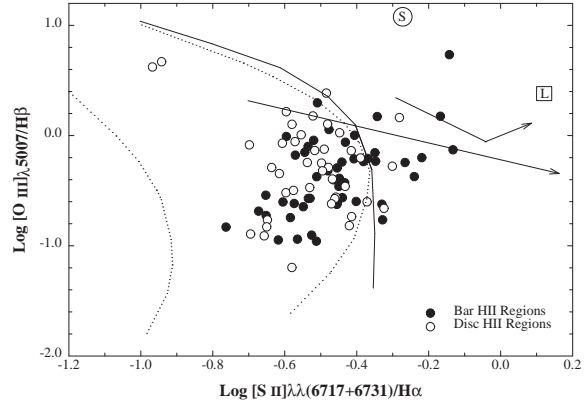


**Fig. 2.** Diagnostic diagram comparing bar and disc H II regions. The dotted lines are the sequence of normal regions defined by Osterbrock (1989) and the full line separates the normal regions from regions which are not exclusively photoionized. The square and circular symbols correspond to the average locations of the Seyfert 2 and LINER galaxies from Rola et al. (1997). The arrows are as in Fig. 1 except that the magnetic field for the top one is 2 μG cm<sup>3/2</sup>

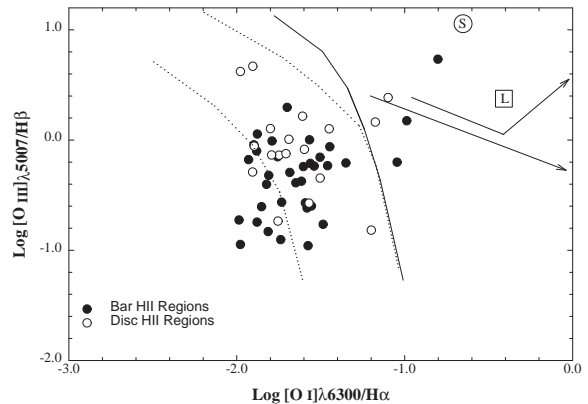


**Fig. 3.** Diagnostic diagram of bar and disc H II regions. The dotted lines indicate the sequence of normal H II regions. The full line is the separation between normal and abnormally excited regions (Osterbrock 1989). The square and circular symbols correspond to the average location of Seyfert 2 and LINER galaxies from Rola et al. (1997). The arrows are as in Fig. 1

### 3.2. Electronic density

The electronic density  $N_e$  in H II regions can be accessed with the line ratio of the [S II] doublet at 6717–6731 Å, i.e.  $\gamma = \frac{[\text{S II}]_{\lambda 6717}}{[\text{S II}]_{\lambda 6731}}$  (Osterbrock 1989). The density can be derived from nebular models published by Blair & Kirshner (1985). Since the calibration depends on the nebu-

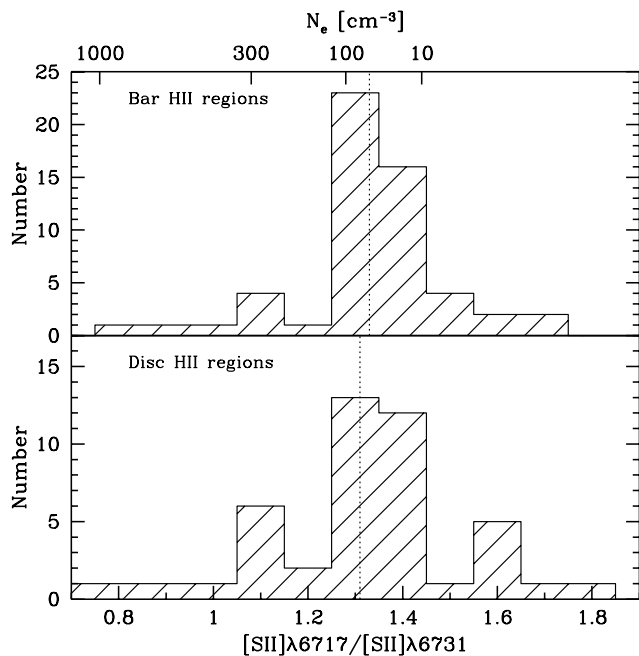


**Fig. 4.** Electronic density distributions for bar (top) and disc (bottom) H II regions. The density conversion derived from the [S II] doublet ratio is from Blair & Kirshner (1985). Vertical dotted lines indicate the mean values

lar temperature ( $N_e \propto T_e^{0.5}$ ), we will assume  $T_e = 10^4$  K. This value is probably too high for the H II regions in our sample with abundances higher than the solar value (see Sect. 3.5). However, for comparison purposes, this approximation is appropriate. The electronic density distributions for the bar and disc H II regions are illustrated in Fig. 4. In both samples, several regions show line ratios that are very close or larger than the low-density limit ( $\gamma \gtrsim 1.4$ ). The electronic densities derived in this regime are very uncertain because the doublet ratio becomes only weakly dependent on  $N_e$  for values larger than about 1.3.

Kennicutt et al. (1989) found that nuclei H II regions tend to possess higher electronic densities on average than disc regions, with both classes showing a large range of densities. As seen in Fig. 4, the case of H II regions located in bars is different. *No significant difference is observed between the distributions of electronic densities of both populations.* On average,  $\gamma \approx 1.33 \pm 0.02$  (bar regions) and  $\gamma \approx 1.31 \pm 0.03$  (disc regions). Bar H II regions do not show any compactness with respect to disc regions.

### 3.3. Extinction

As discussed in the Sect. 2.2, the visual interstellar extinction of individual H II regions can be derived from the  $H\alpha/H\beta$  line ratio. The values derived, however, are approximate since in reality, the real extinction is probably not distributed uniformly but is patchy. Figure 5 presents the distribution of the visual interstellar extinction from

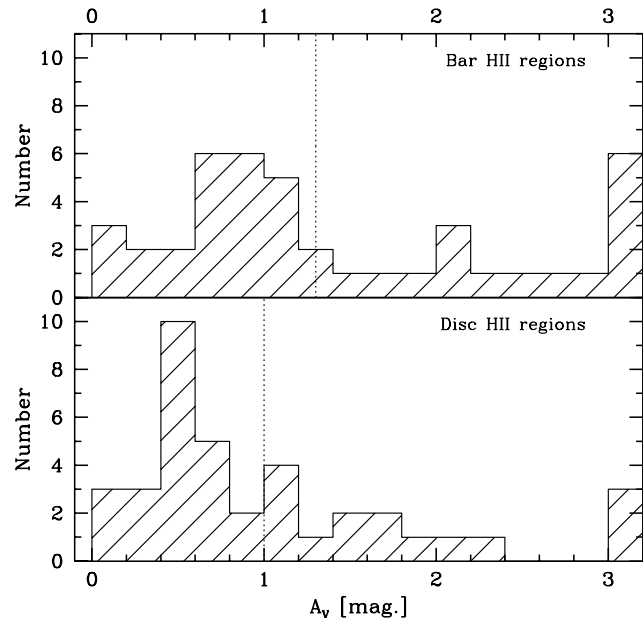


**Fig. 5.** Distributions of the interstellar extinction  $A_V$  derived from the  $H\alpha/H\beta$  line ratio for bar (top) and disc (bottom) H II regions. Vertical dotted lines indicate the mean values

both the bar and disc H II regions. There is a considerable extinction in both populations of H II regions. The mean values are  $A_V \approx 1.3$  and  $A_V \approx 1.0$  visual magnitudes for the bar and disc regions, respectively. This difference is probably not significant since the extinction derived in bar regions, based on the assumption that the nebular temperature is  $10^4$  K, might be overestimated by about 0.1 to 0.2 magnitude.

The extinction values for the bar regions show a large dispersion. Most of the H II regions contributing to the highest values are located in the bars of NGC 7479 and NGC 5921. As noticed in MF97, these regions are located close to the strong dust lanes seen in these bars. Nevertheless, the overall behavior shows that the interstellar extinction as derived from the Balmer decrement is similar for bar and disc regions. However, using IRAS observations, Phillips (1993) has shown that for circumnuclear regions the extinction derived from the  $H\alpha/H\beta$  ratio can be underestimated by as much as 2 magnitudes. The “uniform screen” model assumed for the extinction is probably over-simplistic. Any line ratios (e.g.  $R_{23}$ ) or other quantitative properties (e.g. integrated fluxes) severely affected by the interstellar extinction should be interpreted with caution for regions located in the inner parts of galaxies.

### 3.4. $H\alpha$ equivalent widths

The equivalent widths (EW) of the Balmer emission-lines provide a measure between the number of ionizing and

continuum photons emitted in the H II region. As such, the EWs depend strongly on the stage of evolution of the ionizing stars, the initial mass function (IMF), and the metallicity (Dottori 1981; McCall et al. 1985; Copetti et al. 1986; Bresolin & Kennicutt 1997; Bresolin et al. 1999; Leitherer et al. 1999). As shown by Copetti et al. (1986) and more recently by Leitherer et al. (1999),  $EW(H\alpha)$  and  $EW(H\beta)$  can both be used as age indicators for H II regions. In disc galaxies, the distribution of  $EW(H\alpha)$  extends from about 100 Å to 1500 Å with a median value around 400 Å. No obvious correlation with the Hubble type is found (Bresolin & Kennicutt 1997). Assuming an instantaneous burst of star formation and a solar metallicity, these values correspond to an age range between 1 Myr to 7 Myr (Leitherer et al. 1999).

The accuracy of the Balmer line EWs is mostly determined by the uncertainty in the level of the nebular continuum which is severely contaminated by the galactic continuum. Because we could not directly measure the contribution from the galactic continuum on our “off” band images used in MF97, we have only measured the EWs for the  $H\alpha$  line. The  $EW(H\alpha)$  is also less affected by the interstellar extinction and the underlying absorption. The fraction of the galaxy light contributing to the nebular continuum was estimated from two photometric apertures: one covering the integrated light of the H II regions, and the other located on nearest area devoid of any  $H\alpha$  emission (determined from the  $H\alpha$  images). A correction factor was then applied to the EW values measured directly from the spectra. These correction factors vary from 1.1 to 20 depending on the location of the H II region.

Figure 6 illustrates the  $EW(H\alpha)$  distributions of the bar and disc H II regions. The mean values for the distributions differ by about a factor of two:  $EW(H\alpha) \approx 250$  Å (bar regions) and  $EW(H\alpha) \approx 560$  Å (disc regions). Following the models of Leitherer et al. (1999) for an instantaneous burst of star formation with a Miller-Scalo mass function and solar metallicity, the mean age of bar regions is about 5.3 Myr while disc regions are about 4.0 Myr old. However, the difference in age is less ( $< 1 \times 10^6$  yr) when a Salpeter function is used to describe the IMF. Also, no age gradient seems to exist along the sequence of bar H II regions. This is an indication that H II regions should be ignited all along the bar and not only at bar ends with a subsequent migration towards the center.

In their study of nuclear H II regions, Kennicutt et al. (1989) found that the  $EW(H\alpha)$  of the H II region nuclei, with a median value around 25 Å, are approximately 20 times lower on average than that of normal disc regions. Such a difference cannot easily be explained by assuming that the correction for galactic continuum was underestimated. The authors rather favor the idea that the stellar continuum is high due to continuous star formation in the same region or an unusual stellar mass spectrum in the ionizing clusters. In the present case, however, it is difficult to completely discard the effect of the contamination

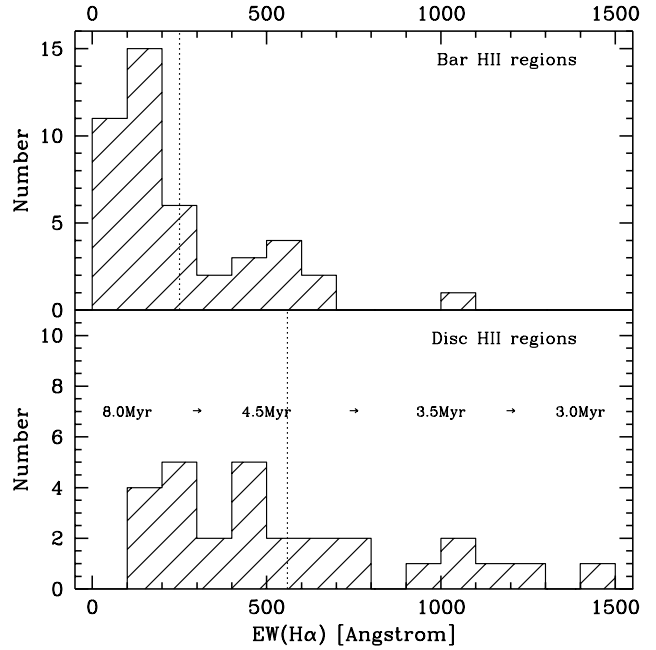


**Fig. 6.** Distribution of the  $H\alpha$  equivalent widths  $EW(H\alpha)$  for the bar (top) and disc (bottom) H II regions. The scale in the bottom panel indicates the approximate age of the H II regions from models with a Salpeter IMF, instantaneous burst of star formation and solar metallicity (see Leitherer et al. 1999 for details). Vertical dotted lines indicate the mean values

of the galactic continuum to the nebular continuum to explain the discrepancy observed between bar and disc regions. The location of the aperture used to measure the galaxy continuum has a strong effect on the correction performed. The light distribution in bars is not uniform and some bars have very patchy dust features. A systematic error of a factor 2 cannot be ruled out. In any case, no firm conclusion based on the difference observed in the  $EW(H\alpha)$  of both populations of H II regions can be drawn from the actual sample.

### 3.5. $O/H$ abundance (within bars)

The oxygen abundance in H II regions can be derived either through semi-empirical calibrations (e.g. Edmunds & Pagel 1984; McGaugh 1991; Pagel 1997) or directly when the temperature can be measured from the nebular lines  $[O I] \lambda 4363$  or  $[N II] \lambda 5755$ . The latter, however, are generally detectable only for H II regions with low oxygen abundance. In our case, almost all the regions have solar or above-solar oxygen abundances; semi-empirical techniques have to be used. Even if the uncertainties related to these methods are generally quite large ( $\pm 0.2$  dex), it is worthwhile to derive the  $O/H$  values to address the important question of mixing of the ISM in bars. It is now well established that bars induce large-scale mixing of the

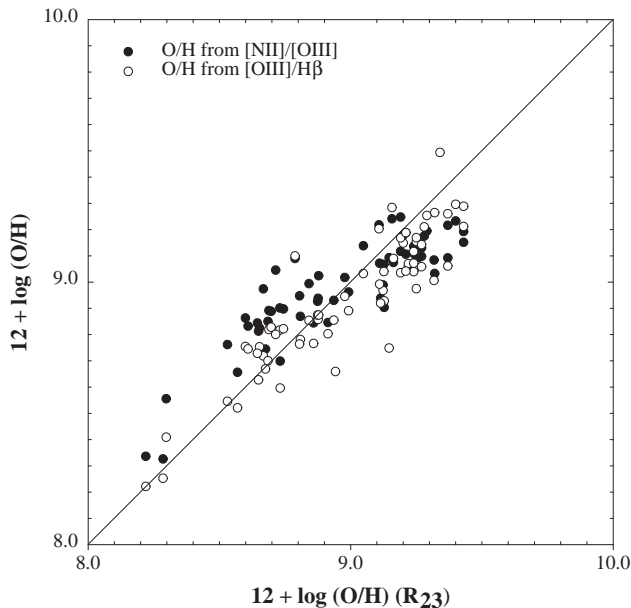


**Fig. 7.** Comparison between the O/H abundances values given by three different line ratios:  $[\text{N II}]/[\text{O III}]$ ,  $[\text{O III}]/\text{H}\beta$ , and  $R_{23}$

chemical composition in the disc of spirals (Martin & Roy 1994; Zaritsky et al. 1994; Friedli et al. 1994). The radial flows of gas formed by bars flatten the strong (negative) abundance gradients generally observed in unbarred late-type disc galaxies. The importance of the homogenization effect is related to the bar strength as shown by Martin & Roy (1994). Very strong gas flows ( $v \gtrsim 100 \text{ km s}^{-1}$ ) are taking place along bars; efficient mixing should be also observed and the O/H scatter between the bar H II regions should be smaller than what is observed in normal galaxy discs (See Sect. 4).

The oxygen abundances for our sample of bar H II regions were determined using three line ratios:  $[\text{N II}]/[\text{O III}]$ ,  $[\text{O III}]/\text{H}\beta$ , and  $R_{23} = \frac{[\text{O II}]_{\lambda 3727} + [\text{O III}]_{\lambda \lambda 4959, 5007}}{\text{H}\beta}$ . The conversion to relative oxygen abundances was done using the calibration of Edmunds & Pagel (1984). Much has been written on the accuracy of these line ratios as abundance indicators (e.g. McGaugh 1991; Martin & Roy 1995; Stasińska 1998). For our sample, Fig. 7 compares the different O/H values derived with all three indicators. The O/H values derived from  $[\text{N II}]/[\text{O III}]$  are slightly higher ( $\sim 0.1$  dex) than the values derived from  $[\text{O III}]/\text{H}\beta$  and  $R_{23}$  for  $12 + \log(\text{O}/\text{H}) < 8.9$ . For  $12 + \log(\text{O}/\text{H}) > 8.9$ , that is, the abundance regime for most of the bars in our sample, the abundances from  $[\text{O III}]/\text{H}\beta$  and  $[\text{N II}]/[\text{O III}]$  are slightly below the values given by  $R_{23}$ . These results were previously discussed by Martin & Roy (1994) and

are due to discrepancies in the semi-empirical calibrations. For our purposes, we use the O/H values derived from the  $[\text{N II}]/[\text{O III}]$  indicator; our conclusions are not affected by this choice.

The distribution of the oxygen abundance along the bars of our sample is illustrated in Fig. 8. It is clear that the O/H scatter observed in these bars is well smaller than  $\pm 0.1$  dex or even less. Martin & Belley (1996, 1997) have shown that the azimuthal O/H dispersion observed in the discs of normal and barred galaxies is generally equal or larger than  $\pm 0.2$  dex. These abundance variations are probably not intrinsic but are in fact a combination of real inhomogeneities and uncertainties associated with empirical techniques (Roy & Kunth 1995). However, a comparative analysis remains possible when the same method is used to derive the O/H values (Martin & Belley 1997). Clearly, the chemical composition of H II regions in a bar is well-homogenized. This indicates that an efficient mixing of the chemical composition is taking place in the bar region (see next section).

#### 4. Discussion

*Degree of ionization.* As discussed in Sect. 3.1, bar H II region spectra do not exhibit any obvious signs of high-velocity shocks or hard UV radiation. However, there is marginal evidence from Figs. 2 and 3 that the ionization might be different for some bar regions. The degree of ionization at a specific position in a nebula can be accessed through the ionization parameter:

$$U = \frac{Q(H^0)}{4\pi r^2 c N_e} \quad (1)$$

where  $Q(H^0)$  is the number of ionizing photons per unit time by the central source,  $r$  is the position in the nebula, and  $c$  the speed of light (Osterbrock 1989). The most obvious evidence that bar regions are different from disc regions is seen in the  $[\text{O I}] \lambda 6300$  line. As described in Evans & Dopita (1985), the  $[\text{O I}]$  line is emitted in the transition zone of an H II region which contains a significant fraction of neutral hydrogen. The line is then stronger when  $U$  is lower (or the ionizing stellar temperature is lower). Since we have detected the  $[\text{O I}]$  line in a much larger fraction of bar regions than in disc regions, this suggests that the ionization parameter could be lower in the former population. Figure 9 shows the correlation between  $[\text{O I}] \lambda 6300/[\text{O III}] \lambda 5007$  and  $[\text{O II}] \lambda 3727/[\text{O III}] \lambda 5007$  which is particularly dependent on  $U$  (Evans & Dopita 1985). A correction for the interstellar extinction has been applied to these line ratios. The bulk of bar H II regions is located at  $U \sim 0.0005$ . For the disc regions, the scatter is quite large but on average  $U \sim 0.001$ , larger than the value for bar regions. Unfortunately, our sample is not large enough to firmly confirm that  $U$  is indeed different for both populations of H II regions.

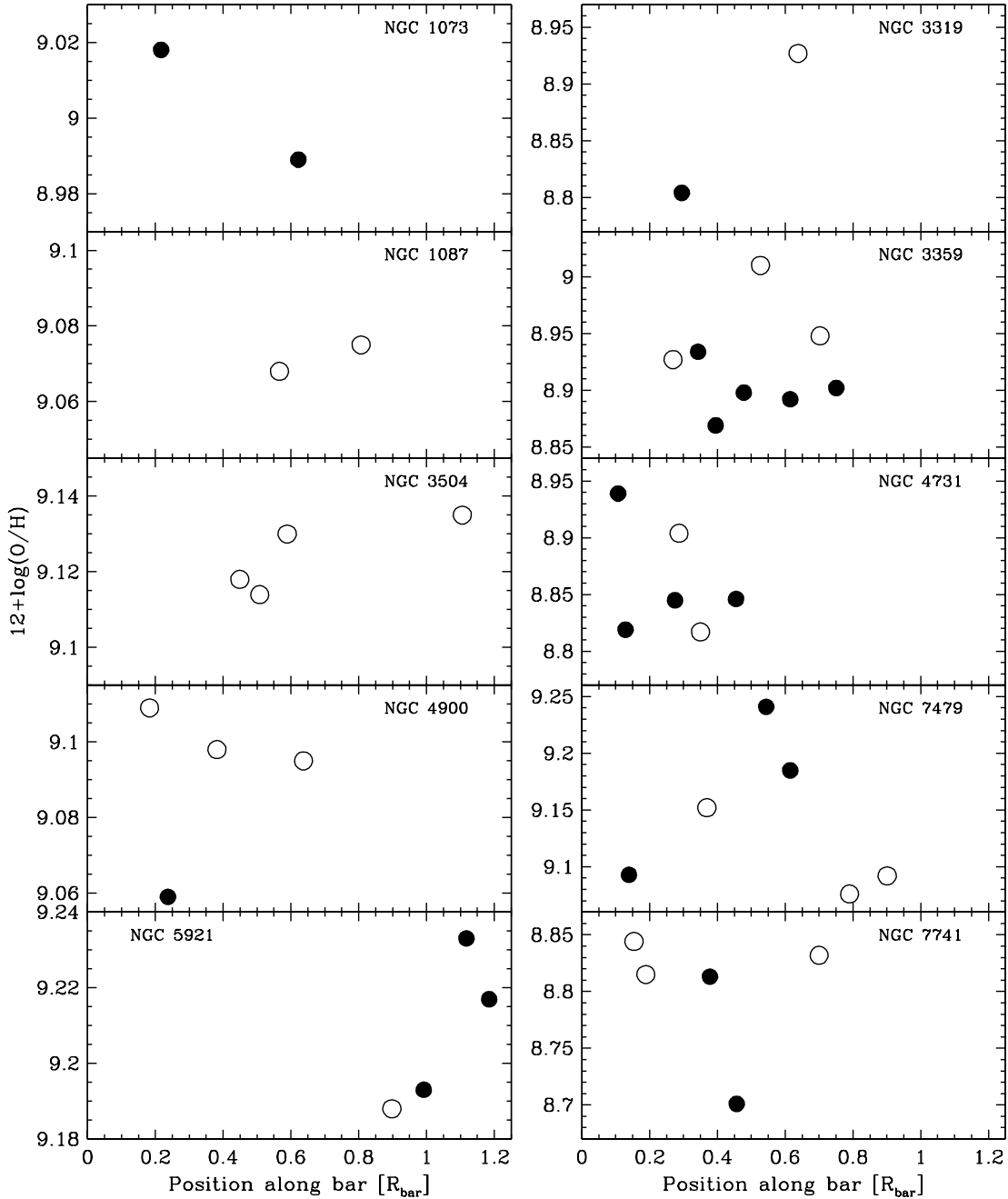


**Fig. 8.** O/H abundance distributions along the bars of the galaxies in our sample. The O/H values were derived using the  $[\text{NII}]/[\text{OIII}]$  line ratio. The horizontal axis is the position of the regions normalized to the bar radius given in MF97. The open and black symbols differentiate the regions with regard to what side of the bar they are located. The abundance interval is 0.06 dex for galaxies displayed in the left column and 0.2 dex for those in the right column

If a difference in the ionization parameter is really present, this could be due to many factors: differences in the initial mass function, age, richness of the OB associations, or spatial distribution of the ionized material (Evans & Dopita 1985). As recently shown by Rozas et al. (1999), the luminosity function (LF) of the bar regions is much less regular than the LF of the disc regions in the

strongly barred spiral NGC 7479. Their result, combined with our study on the nebular excitation, suggest strongly that the properties of the OB associations formed in bars differ from the normal associations of the disc. More work comparing LFs and nebular properties of a larger sample of bar and disc regions would allow us to investigate the origin of this difference. In the final paper in this series



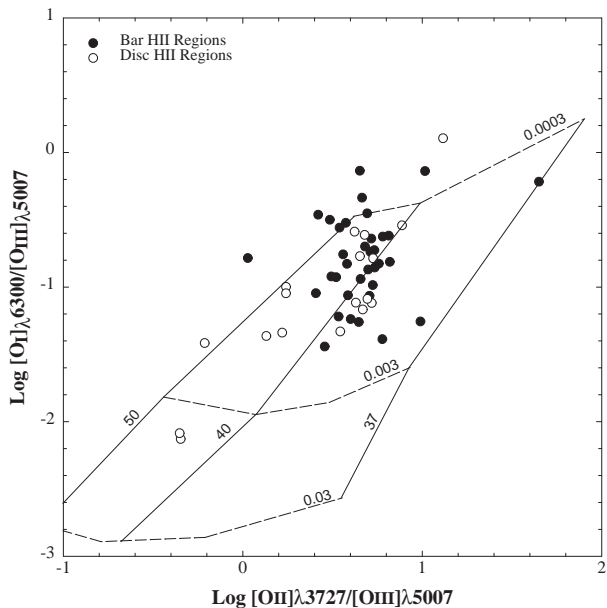


**Fig. 9.** Diagnostic diagram showing the relation between the  $[\text{O I}] \lambda 6300/[\text{O III}] \lambda 5007$  and  $[\text{O II}] \lambda 3727/[\text{O III}] \lambda 5007$  nebular line ratios. Both ratios have been corrected for the extinction. The curves represent models from Evans & Dopita (1985). The horizontal dashed lines show three values for  $U$ , 0.03, 0.003, and 0.0003. The vertical lines indicate the stellar temperatures used in the models, 50 000 K, 40 000 K and 37 000 K.

(Friedli & Martin, in preparation), we will also examine the properties of the clusters formed in diverse bar environments with high-spatial numerical simulations.

*Mixing and element production.* The estimated timescale given by numerical simulations for which the star formation activity phase lasts in bars is  $\tau_{\text{SF}} \sim 5 \times 10^8$  yr (Martin & Friedli 1997). How does this compare with mixing timescale?

It is possible to roughly quantitatively evaluate the timescale of mixing of the ISM due to radial flows. Roy & Kunth (1995) have discussed the diverse mixing mechanisms of the oxygen abundance in the ISM in galaxy discs. Assuming a pure radial mixing due to gas flows funnelled in the bar, the upper limit for the time for gas to diffuse a length scale,  $\Delta x_{\text{rad}}$ , in the radial direction is:

$$\tau_{\text{rad}} = \frac{\Delta x_{\text{rad}}^2}{vl}, \quad (2)$$

where  $v$  is the radial flow velocity, and  $l$  is the mean free path for molecular clouds. In a typical bar,  $\Delta x_{\text{rad}} = 5$  kpc (see Table 1) and  $v = 100 \text{ km s}^{-1}$ . The value of the mean free path for the gas clouds is not a well-defined quantity in bars. In galaxy discs,  $l = 300 - 1000$  pc (Roberts &

Hausman 1984; Roy & Kunth 1995). If we assume  $l = 500$  pc for bars, we find  $\tau_{\text{rad}} \approx 5 \times 10^8$  yr. However, since radial flows in bars are not stationary, the real mixing timescale could be even of the order of  $\tau_{\text{rad}} = \Delta x_{\text{rad}}/v$ , i.e.  $\sim 5 \times 10^7$  yr. Putting all this together yields the following reasonable interval for the mixing timescale:  $5 \times 10^7 \lesssim \tau_{\text{rad}} \lesssim 5 \times 10^8$  yr. Thus,  $\tau_{\text{rad}}$  is shorter than  $\tau_{\text{SF}}$  meaning that the abundance content in H II regions formed during this phase must be homogenized.

It is also instructive to make rough (i.e. close-box) estimates of the global abundance increase during  $\tau_{\text{SF}}$  as well as of the abundance fluctuations in H II regions which should result from their age spread. If  $Z^i$  is the initial mean gaseous abundance in the bar region,  $\epsilon$  the global star formation efficiency, and  $Y_Z$  the net yield for the species considered, then the final mean abundance is given by:

$$Z^f = Z^i + \epsilon(1 - \epsilon)^{-1}Y_Z. \quad (3)$$

Interestingly enough,  $Z^f$  does not depend on the initial gas mass fraction. For instance, for the oxygen with an yield  $Y_O \approx 0.006$ , an initial solar abundance  $Z^i \approx 0.01$ , and a typical SF efficiency  $\epsilon \approx 0.25$ , then  $Z^f \approx 0.012$ . The global increase of oxygen abundance is thus only about 0.1 dex. Equation 3 can in fact also be applied to each individual H II regions with exactly the same numbers; the fluctuations in the oxygen abundance are thus expected to be of the order 0.1 dex, which is indeed what is observed (Sect. 3.5). However, we do not observe any clear trend between the age and metallicity for bar H II regions. In dwarf galaxies, the metal enrichment of H II is not observed and metals are probably locked in the hot phase. (see e.g. Tenorio-Tagle 1996; Kobulnicky 1998). The situation could be similar for star forming regions in bars.

## 5. Summary

The main results concerning the properties of H II regions located within bars can be expressed as follows:

- 1) From standard diagnostic diagrams, the excitation of most H II regions appears normal and similar to the one of disc regions. There are some exceptions for nuclear regions where an ionization mechanism other than photoionization seems to be present. However, there is marginal evidence that the ionization parameter in bar regions is lower than in disc regions, suggesting that the properties of the OB associations might be different in bar environments.
- 2) The electronic density distribution as derived from the  $[\text{S II}]$  line ratio is similar to that observed for normal disc regions. The mean density is  $N_e \approx 80 \text{ cm}^{-3}$ . Star formation regions in bars have the same ‘‘compactness’’ as disc regions.
- 3) The  $H\alpha/H\beta$  extinction indicator reveals that, on average, bar regions have a visual extinction  $A_V \sim 1.3$  mag,

*0.3 mag more than disc regions.* This difference is mainly due to the fact that some regions are located near the bar dust lanes of the earlier types of galaxies in our sample.

4) *The average H $\alpha$  equivalent width for the bar regions is about 250 Å, half that of disc regions.* While this could indicate an older population for bar H II regions, the corresponding age difference is probably too small to be significant owing to the large uncertainties introduced by the galactic continuum correction.

5) *The O/H abundance distribution of these H II regions is remarkably homogeneous.* This is the result of the gaseous radial flows in bars inducing mixing of the ISM, as seen on a larger scale in the discs of barred spirals.

*Acknowledgements.* Discussions with P. Ferruit, L. Binette, R. Kennicutt, and J.-R. Roy were most appreciated throughout this work. We also thank the referee, Françoise Combes, for her helpful comments. The efficient support offered by the technical staff of the Multiple Mirror Telescope during the observations was much appreciated. This work was supported by NSERC (Canada), FCAR (Québec) and in part by the NSF through grant AST-94-21145. D.F. acknowledges the kind hospitality of CFHT.

## References

- Baldwin J., Philips M., Terlevich R., 1981, PASP 93, 5  
 Blair W.P., Kirshner R.P., 1985, ApJ 289, 582  
 Bresolin F., Kennicutt R.C., 1997, AJ 113, 975  
 Bresolin F., Kennicutt R.C., Garnett D.R., 1999, ApJ 510, 104  
 Copetti M.V.F., Pastoriza M.G., Dottori H.A., 1986, A&A 156, 111  
 Dopita M.A., Sutherland R.S., 1995, ApJ 455, 468  
 Dottori H. A., 1981, Astrophys. Space Sci. 80, 267  
 Edmunds M.G., Pagel B.E.J., 1984, MNRAS 211, 507  
 Evans, I. N, Dopita, M. A., 1985, ApJS 58, 125  
 Friedli D., Benz W., 1995, A&A 301, 649  
 Friedli D., Benz W., Kennicutt R.C., 1994, ApJ 430, L105  
 García-Barreto J.A., Franco J., Carrillo R., Venegas S., Escalante-Ramírez B., 1996, RevMexAA 32, 89  
 Kennicutt R.C., Keel W.C., Blaha C.A., 1989, AJ 97, 1022  
 Kobulnicky H.A., 1998, in Abundance Profiles: Diagnostic Tools for Galaxy History, ASP Vol. 147, eds. D.Friedli et al. (San Francisco: ASP), 108  
 Leitherer C., Schaerer D., Goldader J.D., et al., 1999, ApJS, in press  
 Martin P., Belley J., 1996, ApJ 468, 598  
 Martin P., Belley J., 1997, A&A 321, 363  
 Martin P., Friedli D., 1997, A&A 326, 449 (MF97)  
 Martin P., Roy J.-R., 1994, ApJ 424, 599  
 Martin P., Roy J.-R., 1995, ApJ 445, 161  
 Martinet L., Friedli D., 1997, A&A 323, 363  
 McCall M.L., Rybski P.M., Shield G.A., 1985, ApJS 57, 1  
 McGaugh S.S., 1991, ApJ 380, 140  
 Osterbrock D.E., 1989, Astrophysics of Gaseous Nebulae and Active Galactic Nuclei (Mill Valley: Univ. Science Books)  
 Pagel B.E.J., 1997, Nucleosynthesis and Chemical Evolution of Galaxies, (Cambridge: Cambridge Univ. Press)  
 Phillips A.C., 1993, Ph.D. Thesis, Univ. of Washington, USA  
 Phillips A.C., 1996, in Barred Galaxies, ASP Vol. 91, eds. R. Buta et al. (San Francisco: ASP), 44  
 Roberts W.W., Hausman M.A., 1984, ApJ 277, 744  
 Rola C.S., Terlevich E., Terlevich R.J., 1997, MNRAS 289, 419  
 Rozas M., Zurita A., Heller C.H., Beckman J.E., 1999, A&AS 135, 145  
 Roy J.-R., Kunth D., 1995, A&A 294, 432  
 Stasińska G., 1990, A&AS 83, 501  
 Stasińska G., 1998, in Abundance Profiles: Diagnostic Tools for Galaxy History, ASP Vol. 147, eds. D.Friedli et al. (San Francisco: ASP), 142  
 Savage B.D., Mathis J.S., 1979, ARA&A 17, 73  
 Tenorio-Tagle G., 1996, AJ 111, 1641  
 Veilleux S., Osterbrock D.E., 1987, ApJS 63, 295  
 Zaritsky D., Kennicutt R.C., Huchra J.P., 1994, ApJ 420, 87